1.0 SUBJECT /OBJET

The present technical note aims at providing a comprehensive biological analysis of the local tissue effects and the performance of a dental implant presenting micro/nanofeatures through the Starsurf® surface treatment. Such assessment is conducted through sheep femoral implantation *in vivo*, and through histopathologic, histomorphometric and micro-computed tomography analyses.

2.0 SCOPE / DOMAINE D'APPLICATION

This technical note is included into the Starsurf® validation project.

3.0 REGULATORY AND NORMATIVE REFERENCES / REFERENCES REGLEMENTAIRES ET NORMATIVES

— OECD series on Good Laboratory Practice and compliance monitoring number 1, ENV/MC/CHEM(98) 17, on January 26, 1998 for non clinical safety testing on pharmaceuticals, pesticides, food, and feed additives, cosmetic products, veterinary drug products and similar products and industrials chemicals adopted by Council decision on November 26,1997, Directive C (97) 186 final.

— 21 CFR 58 (current version) Food and drugs - United States FDA Department of health and human services. Good Laboratory Practice for non clinical laboratory studies.

— International Organization for Standardization (ISO) 10993: Biological Evaluation of Medical Devices - Part 2: Animals welfare requirements (2006) - Part 6: Tests for Local Effects after Implantation (2016) - Part 12: Sample preparation and reference materials (2012).

— European Directive 2010/63/EU regarding the Protection of Animals used for Scientific Purposes (2010).

4.0 TERMINOLOGIES AND ABBREVIATIONS / TERMINOLOGIES ET ABREVIATIONS

- NA -

5.0 EQUIPMENT-MATERIALS-SAMPLES / EQUIPEMENTS – MATERIELS – ECHANTILLONS

- NA -

6.0 TESTS

Material and Methods, results and their discussion are included in « Appendix I — White paper STARSURF » of the present technical note.

7.0 CONCLUSION

The present study demonstrates that the Starsurf® surface treatment, generating a combination of micro- and nanofeatures on the surface of a titanium implant, has significant beneficial effects on the osseointegration process. Such treatment suggests an increase in the kinetics of bone regeneration and remodeling to the extent that original bone architecture is recovered within 13 weeks, allowing the long-term implant stability. Furthermore, such osseointegration occurs without any deleterious local effect on the surrounding tissue, showing a good compatibility of the implant within its environment. Finally, the distinction between the coronal and apical regions of the implant allowed to demonstrate a difference of bone behavior along the implant, that could be both attributed to the change of implant thread geometry and increasing mechanical stresses generated at the apex.

8.0 APPROVALS / VALIDATION DU DOCUMENT

Date		Name / Position Nom / Fonction	VISAS
06/02/2020	Written by: N.ROUSSEAU Rédigé par :	PhD Student - R&D Engineer	*Rousseau*
06/02/2020	Approved by: A. CHORIER Validé par :	Medical Device Intelligence Director – Quality, Validation and Regulatory Affairs	*horier*

9.0 APPENDICES / ANNEXES

- Appendix I – White Paper STARSURF

Synergistic effects of endosseous implants micro- and nanotopography for bone original architecture recovery
An *in vivo* study in the sheep

Abstract

Surface chemical and topography modifications are currently of major interest to improve osseointegration and long-term success of dental implants. Very few studies assess the performance of implants presenting both micro- and nanofeatures *in vivo* and for animal models used in the context of preclinical studies for medical device certification. This study intends to evaluate the local effects of such implant compared to one of identical design and material without surface treatment. Implants surfaces are characterized in terms of topography, surface chemical composition, roughness and wettability. After 4 weeks and 13 weeks of implantation in sheep, a total of forty implants performance is evaluated through micro-computed tomography, histopathological and histomorphometric analyses. No adverse effect was observed around implants. Histomorphometric analyses indicate that resulting bone-to-implant contact in the coronal region of the surface treated implant is significantly higher at week 4 and week 13, reaching respectively $79.3\pm11.2\%$ and $86.4\pm6.7\%$, than the implant without surface treatment, reaching respectively $68.3\pm8.8\%$ and $74.8\pm13\%$. Micro-CT analyses revealed different healing patterns between the coronal and apical regions, with higher bone-to-implant contact for the coronal one at week 13. Histopathological results indicate at week 13 that bone around the surface treated implant recovered its original architecture while the implant without surface treatment still presents bone condensation and traces of the initial drill defect. Such results suggest that the surface treated implant, in addition of not being deleterious for local tissues, promotes faster regeneration and remodeling of bone around the implant towards peri-implant bone original architecture recovery.

Keywords : osseointegration; dental implants; bone remodeling; nanostructures; surface treatment; sheep model

1 Introduction

Teeth replacement by a dental implant is nowadays a common procedure for the oral rehabilitation of partially or fully edentulous patients. Such success is the result of the discovery of a phenomenon termed osseointegration, a direct bone-to-implant contact establishment that leads to a functional connection and a load transfer between the two components. This concept was introduced for the first time in the late 1960s by Branemark et al. (1969) and by Schroeder et al. (1976) [1, 2], who used the term to refer to a clinical state rather than an implant property. Ever since, researchers and industrials goal focus on the constant provision of new ways to improve the osseointegration process and to maintain dental implants well-integrated in bone in the long term. Prerequisites for implants osseointegration include (1) a minimal trauma inflicted during surgery, (2) the establishment of bone anchoring (referred as primary stability and greatly influenced by implant design), (3) the avoidance of local infections and implant micro-movements. Dental implants osseointegration is then the result of a cascade of biological events. First, proteins contained in blood are adsorbed at the surface of the implant. This phe-

nomenon triggers the adhesion and activation of red blood cells, platelets and inflammatory cells to secrete cytokines, growth and differentiation factors, resulting in the formation of a blood clot that acts as a scaffold for the migration of mesenchymal stem cells and osteoblasts towards the implant. These cells, under the influence of growth and differentiation factors, deposit a new and condensed collagenous matrix that forms woven bone, generating a continuity at the bone-implant interface. This formation occurs both from the host bone cavity towards the implant surface and inversely : we respectively talk about distance osteogenesis (osteoinduction) and contact osteogenesis (osteoconduction). Then, woven bone is progressively remodeled into lamellar bone, showing higher degrees of mineralization and providing a stronger fixation of the implant.

It is accepted by the scientific literature that implants surface modifications, in terms of chemical composition and topology, have an impact on their rate of osseointegration. Indeed, *in vivo* studies demonstrate that features introduced at the micrometric scale on titanium surfaces, in comparison with smoother surfaces, enhance bone-to-implant contact (BIC) 8 weeks following implantation [3–6]. *In vitro* stud-

ies are in accordance with such observations, reporting a decrease of osteoblasts at the interface of bone with rough surfaces, in favor of an increase of differentiation markers such as alkaline phosphatase and osteocalcin [5, 7–10]. Osteoblasts are leaving earlier their proliferation phase to enter the differentiation one, maturing faster and quickly starting to secrete extracellular matrix (ECM). On the other hand, surfaces presenting nanofeatures have shown *in vivo* an improved BIC and a higher implant removal torque, two weeks after implantation [11, 12], as well as a better adhesion of osteoblasts *in vitro* [13, 14]. It is to notice that the combination of micro-features and nanofeatures generates synergistic effects of both topographic levels, in addition to a drastic increase of surface hydrophilicity [15–18]. To our knowledge, very few in vivo studies were conducted to assess the synergistic influence of micro and nanofeatures on dental implant osseointegration [19–21]. As a matter of fact, such studies have only been conducted either on small animals [19, 21], or for very short periods [20]. Recently, by studying screw-shaped cylinders implanted during three months in osteoporotic sheep mandibulars, Liu et al. (2019) demonstrated higher biomechanical parameters for surfaces presenting micro/nanofeatures [22]. However, no assessment of the neo-bone formation, of fibrosis, nor of the bone texture was conducted in this study. Furthermore, for all mentioned studies no distinction was made between the coronal area and the apical area of the implant. Consequently, no behavior difference can be observed in the osseointegration of the two distinct area, questioning the local influence of implants design features.

The purpose of this paper is to provide a comprehensive biological analysis of the local tissue effects and the performance (osseointegration and osteogenesis) of a dental titanium implant presenting micro/nanofeatures. Therefore, sheep were implanted with dental implants of a unique design, treated or not with Starsurf®, a chemical surface treatment developed and commercialized by Selenium Medical (La Rochelle, France), that aims at introducing micro/nanofeatures at the surface of the implant [23, 24]. A total of eight sheep were bilaterally implanted in the medial femoral condyle and terminated four weeks and thirteen weeks after implantation. This model was used in intraosseous implantation studies which were published in scientific peer-reviewed journals and is recognized by International Regulatory Organisms [25, 26]. Furthermore, sheep femoral implantation model is highly standardized and associated with low rates of complication. The osseointegration properties of dental implants can be assessed with minimal variability, ensuring finer comparisons than with jawbone implantation. Finally, sheep model have the advantage of having a body weight as well as bone healing and remodelling patterns more similar to humans than small animals [27]. In addition to surface topography qualitative characterization and chemical composition assessment, the local tissue effects and the performance of the endosseous implants were evaluated through histopathologic, histomorphometric and micro-computed tomography analyses at each time period. Quantitative information is given both for the coronal region and the apical region of the implant.

2 Materials and method

2.1 Ethical Statement

The implantation protocol was approved by the Namsa Ethical Committee (Chasse-sur-Rhône, France). It is part of a project authorization that is reviewed every five years by the French Ministry of Education, Higher Education and Research. The different surgical procedures and biological analyses were conducted by the Medical Research Organization Namsa (Chasse-sur-Rhône, France) [28, 29], in compliance with the OECD series on Good Laboratory Practice and compliance monitoring and FDA 21 CFR 58 on Good Laboratory Practice (GLP) for non clinical studies. The study design was also based on the ISO 10993-6, Biological Evaluation of Medical Devices Part 6 (2016): Tests for Local Effects after implantation. The animal study was conducted in accordance with the ARRIVE guidelines [30]. The relevancy of the animal selection and its use were carefully established and considered.

2.2 The device

Forty-eight commercially available implants and made from commercially pure titanium (cpTi, grade IV) were implanted during this study (Fig. 1), including eight reserves implants. These last were treated similarly as the forty other ones and only intended for replacement in case of adverse event.
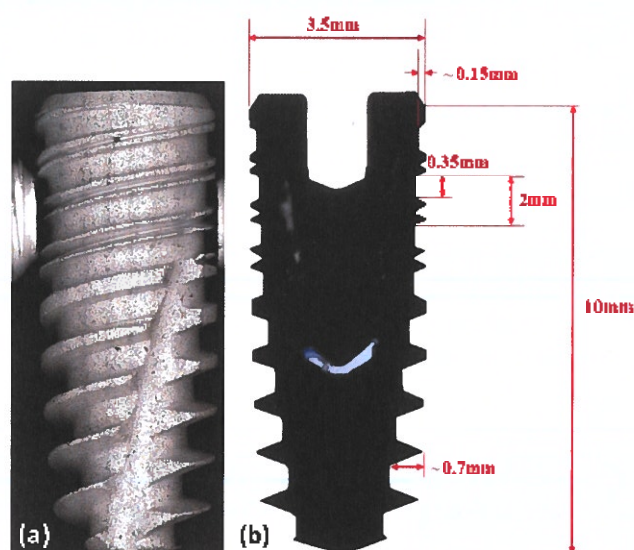

Figure 1: (a) Full-Size High-Resolution SEM image of the dental implant used for the study; (b) General dimensions of the device.

The intra-osseous part of the implant has a diameter of 3.5 mm, a length of 10 mm and is composed of a cylinder part (coronal area) and a conical one (apical area). The main thread is composed of a double fillet with a pitch of 2 mm. Considering the conical aspect of the implant, the thread depth is increasing from approximately 0.15 mm in the coronal zone to 0.7 mm in the apical one. In the coronal zone, the main thread is subdivided into two "micro" fillets of same pitch. Such implant geometry is common and representative of implants that are currently on the market [31]. Two configurations are tested in this study : a standard topography (REF, n= 10 + 2 reserves at both 4 weeks and 13 weeks time-periods) and a Starsurf® one (TEST, n= 10 + 2 at both 4 weeks and 13 weeks time-periods), composed of a micro/nanofeatures combination. The standard topography is obtained through corundum sandblasting while the Starsurf® one is a succession of mechanical and chemical treatments. First, implants are sandblasted using a mixture of hydroxyapatite (HA) and β-tricalcium phosphate (β-TCP). Then, an acid attack is conducted with hydrochloric and sulfuric acid. Finally, a basic attack is conducted using potassium hydroxide. Cleaning in clean rooms, sterile packaging and final gamma irradiation was applied on both series of implants prior implantation. Following implantation the threads are engaged in the host bone cylindrical wall obtained after drilling, providing primary mechanical stability of the device.

2.3 Implant surface characterization

Under a Captair Flow 468 ISO5 laminar flow hood (Air-Lab), the overall topography of REF and TEST implants was qualitatively examined using Phenom ProX Scanning Electron Microscope (ThermoFisher scientific). Micrographs at different magnification were observed for the assessment of the topographies at different scales. Then, the surface chemical composition was assessed by Energy Dispersive X-Ray Spectrometry (EDX). Roughness measurements have been conducted on cpTi discs with and without Starsurf® using interferometry. Such technique allows to extract the main roughness parameters of the examined surface (Sa, Sz, Sq, Sp, Sv). Three samples for the REF and TEST surfaces have been measured, with a characterized area of 24mm². Finally, REF and TEST surfaces wettability has been tested through contact angle measurements on the same discs. Surface free energy is assessed using Owens-Rankine formulation, with three liquids (water, ethylene glycol and diiodomethane), droplets of $2\mu l$ and 8 contact angle measurements per liquid.

2.4 Study design and experimental animals

Animal model and management

Eight (n= 4 per time-period) female Blanche du Massif Central sheep (Bergerie de la Combe aux Loups, France) were involved in the study. Sheep were aged from 2 to 4 years (mean= 2.7 years), skeletally mature, and weighted from 57 to 68 kg at implantation (mean= 61.25 kg). The sheep is an animal model identified for evaluating materials and is recommended in the ISO 10993 standard - part 6 (2016) for intraosseous implantations. Sheep were bilaterally implanted in the medial femoral condyle. The use of sheep femurs allows to implant up to three screw-type implants per leg, to increase the number of sites per implant group, without increasing the number of animals. Sheep were randomly attributed to the two periods of implantation studied and the number of sites per implant group were chosen to be compliant with the ISO 10993 standard - part6. One implant group per condyle was implanted, to allow a suitable evaluation of the local tissue effects and performance, and to avoid tissue response between implant groups. Husbandry, housing and environment conditions were conformed to the European Directive 2010/63/EU regarding the protection of animals used for scientific purposes. Animals were housed at Namsa, AAALAC international accredited facility and registered with the French Department of Agriculture for animal housing, care and investigations. Groups were organized in cages identified by a card indicating the study number, animal numbers, sex, dates of beginning and end of experimental in-life phase. Animals were kept under laboratory conditions. The animal housing room temperature and relative humidity were recorded daily. The recommended temperature range for the room was 10 - 24°C and the light cycle was controlled using an automatic timer (12 hours of light, 12 hours of dark). After the post-operative period, the sheep of the 13-week group were group housed in a farm setting (Bergerie de la Combe aux Loups, France). During the farm setting, the environmental conditions were not controlled. Standard hay was provided *ad libitum* and supplemented with a commercially available pelleted sheep feed (Special Diet Services, France). Minerals were provided *ad libitum* (Sodimouton, Salins Agriculture). Potable water was delivered *ad libitum* through species appropriate containers or delivered through an automatic watering system.

Pre-operative procedure

On the day of surgery, pre-medication was performed by intravenous injection of a mixture of diazepam (Diazepam®, TVM) and butorphanol (Torphasol®, Axience). Anesthesia was induced by intravenous injection of propofol (Propovet®, Zoetis). Each sheep was intubated, mechanically ventilated and placed on isoflurane inhalant anesthetic (IsoFlo®, Zoetis) for continued general anesthesia. An intravenous infusion with suitable electrolyte solution (Ringer lactate, Baxter) was performed during surgery. Pre-operative injection of an anti-inflammatory drug (carprofen, Rimadyl®, Zoetis, subcutaneous) and a prophylactic antibiotic treatment (amoxicillin, Duphamox LA®, Zoetis, intramuscular) were administered. The surgical areas were clipped free of wool, scrubbed with povidone iodine (Vetedine savon®, Vetoquinol), wiped with 70% isopropyl alcohol (Savetis), painted with povidone iodine solution (Vetedine solution®, Vetoquinol) and draped. The sheep were placed in the supine position on a warmed
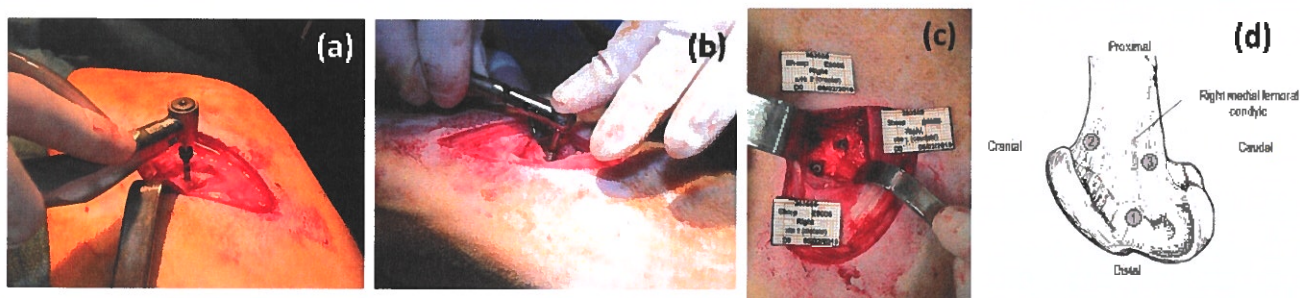
Figure 2: Surgery procedure for implantation. (a) Drilling operation at 1200 rpm; (b) dental implant insertion at 45 N.cm; (c,d) implants localization on femoral condyle after completed surgery. Three sites per condyle are allocated for implants.

Surgical procedure

pad. A rectal temperature probe and a rumen tube were placed during surgery. Electrocardiogram (ECG), peripheral non-invasive arterial blood pressure and oxygen saturation were monitored. The surgery was performed in a dedicated operating surgical theatre by a surgeon from Namsa, using standard aseptic techniques (Fig. 2). A cutaneous incision was made on the medial side of each femoral condyle. The muscles were separated using blunt dissection to access the femur and the periosteum was carefully removed from the femoral epiphysis to expose implants sites. For each site, four steps of drilling were conducted perpendicular to the bone surface, in order to get a final hole of 3.5 mm diameter with an approximate depth of 10 mm. Each drilling step was conducted with a maximum drilling speed of 1200 rpm and followed by extensive rinsing with saline to control temperature increase at the implantation site and to remove bone debris. Following the drilling steps, each implant was inserted with a maximum torque of 45 N.cm. Incision was closed by suturing separately the capsule, muscles and the subcutaneous layer with absorbable thread (Ethicon® PDS™ II 1 and Ethicon® Coated Vicryl™ 2-0). The skin layer was closed using surgical staples (Appose™ ULC Auto Suture™, Covidien™). The wounds were disinfected using an iodine solution. The operated legs were not restrained in any manner.

Post-operative and terminal procedures

Animals were observed daily for general health and to detect mortality and morbidity. The implantation sites were examined daily for adverse reactions until sutures removal. When any animal exhibited adverse clinical signs, it was examined and treated as need. An intramuscular injection of buprenorphine (Buprecare®, Axience) was administered at the end of the surgery day, then daily for two days post-surgery. An anti-inflammatory drug (carprofen, Rimadyl®, Zoetis) was subcutaneously injected daily for five days post-surgery and antibiotic (amoxicillin, Duphamox LA®, Zoetis) was intramuscularly injected every two days for eight days following surgery. The wounds were disinfected with iodine solution (Vetedine solution®, Vetoquinol) daily until two

days after the removal of the surgical staples. The surgical staples were removed after complete healing (2 weeks following surgery). On week 4 and week 13, the designated animals were weighed and euthanized by an intravenous injection of a lethal solution (Doléthal®, Vetoquinol). These time periods were chosen to evaluate the local tissue effects and the bone healing performance after a short and midterm implantation as recommended in ISO 10993 standard - part 6, for non-degradable materials. The distal femur was harvested and explants were fixed in 10% Neutral Buffered Formalin (NBF) for histopathologic analysis. If not used for replacement, reserve implants sites were harvested the same way, fixed, dehydrated, embedded and stored for eventual subsequent analyses. In order to mark the newly formed calcified mineralization fronts by fluorescence, subcutaneous injections in the neck and the back were conducted beforehand, using three fluorochromes : xylenol orange (XO), calcein green (CG), oxytetracyclin (OTC). For the 4-week group, these fluorochromes were respectively injected at day 5, day 15 and day 25. Injection at respectively week 4, week 8 and week 12 were made for the 13-week group.

2.5 Micro-Computed Tomography (Micro-CT)

Micro-CT preparation

After fixation in 10% NBF (VWR), a total of forty implanted sites, one non-implanted REF article and one non-implanted TEST article were scanned by cone beam micro-computed tomography (μCT 40, SCANCO, Switzerland). The specimens were placed in cylindrical holders to obtain transverse tomograms of the implanted article. The measured data were filtered using a Gaussian filter with finite filter support and filter width. The images were then segmented to separate the implant and bone from the background.

Micro-CT evaluation

Two Volumes Of Interest (VOI) were defined (Fig. 3a). Each VOI consisted in a conical tube with the inner edge along the core of the article (excluding the core but including the threads) and the outer edge placed at a fixed distance
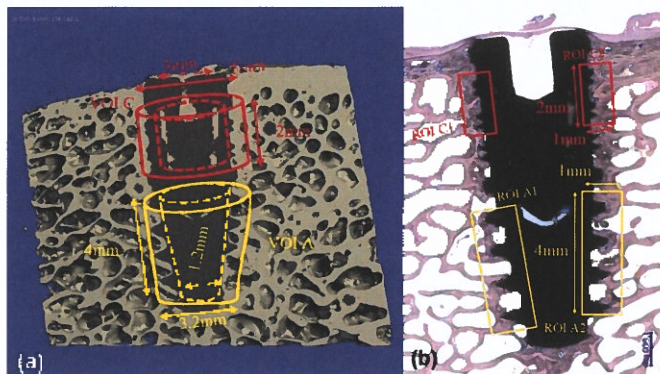
Figure 3: (a) Tomogram obtained by Micro-CT tomography, presenting the different Volume Of Interest (VOI A and C); (b) Representative photomicrograph used for histopathologic analysis, introducing four Regions of interest (ROI A1, A2, C1 and C2).

of 1 mm from the inner edge. The upper VOI (VOI C) was placed in the coronal area of the article. The lower VOI (VOI A) was placed along the apical and conical remaining area of the article. For each VOI, computation of Bone Volume (BV), Bone Volume/Total Volume (BV/TV) and Bone-to-Implant Contact (BIC). The non-implanted scanned implants served as a baseline to help distinguish the article from the bone.

2.6 Histopathology

Histologic preparation

After fixation in 10% NBF (VWR), a total of forty implanted sites, one non-implanted REF article and one non-implanted TEST article were dehydrated in alcohol solutions of increasing concentration, cleared in xylene and embedded in polymethylmetacrylate (PMMA). For each explant and non-implanted article, one central longitudinal section was obtained by a microcutting and grinding technique (Exakt^{TM}, approximately 40 μm thickness). The section was left unstained for epifluorescence analysis and then stained with modified Paragon for qualitative and semi-quantitative histopathologic analysis and for quantitative histomorphometric analysis.

Histopathologic evaluation

Qualitative and semi-quantitative histopathologic evaluation of the local tissue effects at the implantation sites were conducted according to the standard (ISO 10993 – part 6). Tissue damage, cellular inflammatory response, repair phase of inflammation, fatty infiltrate and other parameters such as hemorrhage, cell degeneration, bone ingrowth, encapsulation and bone healing were evaluated semi-quantitatively and graded as described in Appendix A.

Histomorphometric evaluation

The histomorphometric analysis was conducted on forty modified Paragon sections. Sections were scanned (Zeiss AXIOSCAN Z1, x20) and analyzed with a color image ana-

lyzing system (Tribvn, France, CALOPIX 3.2.0) to perform a semi-automatic analysis. Four standardized Regions Of Interest (ROI C1, C2, A1, A2) were defined for each longitudinal section (Fig. 3b). Each ROI consisted in rectangle with the inner edge along the core of the article (excluding the core but including the threads) and the outer edge placed at a fixed distance of 1 mm from the inner edge. The upper ROI (ROI C) was placed in the coronal area of the article. The lower ROI (ROI A) was placed along the apical and conical remaining area of the implant. Each zonal ROI (sum of the ROI C1 and C2 and sum of the ROI A1 and A2) of the TEST was compared to each corresponding ROI of the REF.

2.7 Statistical analyses

Minitab 19 was used to conduct statistical analyses. Student's t-tests are used for comparisons of the two implants. Statistical significance is reached when the P-value is inferior to 0.05 ($\alpha = 0.05$).

3 Results

3.1 Implant surface characterization

Scanning electron microscopy

SEM micrographs of the implant's surface revealed significative differences between the samples topographies. While the REF surface only shows a heterogeneous microtopography (Fig. 4a and 4b), the TEST one had its topography entirely replaced by a homogeneous nodule-like microstructure (Fig. 4c). Furthermore, the nanotopography is visible as a spike-like structure (Fig. 4d).

Energy dispersive X-Ray spectrometry

The EDX spectra revealed very few changes in the chemical composition of the implant after surface treatment (Table 1). Both REF and TEST surfaces are composed of oxygen, titanium and carbon. A slight concentration of aluminium is measured on the REF surface while undetected on the TEST one.

Table 1: Semi-quantitative results of Energy Dispersive X-ray spectroscopy

	Oxygen	Titanium	Carbon	Aluminium
	Atomic Concentration (%)			
REF	45.35	39.33	11.93	3.40
TEST	63.23	27.37	8.38	–

Roughness and contact angle measurements

The roughness surface parameters analysis revealed significative differences between assessed topographies. The roughness parameters indicate that the surface generated by the Starsurf® surface treatment is rougher than the surface obtained through machining. The arithmetical average

(Sa), maximum height (Sz), root mean squared (Sq), maximum peak height (Sp) and maximum valley depth (Sv) are summarized in Table 2.

Table 2: Topographic analysis of roughness generated by surface treatment; values obtained by interferometry.

		Sa	Sz	Sq	Sp	Sv
REF	Mean (μm)	0.33	4.92	0.40	3.00	1.92
	SD (μm)	*0.18*	*2.19*	*0.21*	*1.87*	*0.46*
TEST	Mean (μm)	3.54*	40.99*	4.46*	20.72*	20.27*
	SD (μm)	*0.20*	*2.29*	*0.24*	*1.98*	*1.44*

* $p<0.01$ compared to REF surface.

Contact angle measurements revealed a similar trend, as the TEST surface presented significantly lower contact angles for every liquid than for the REF one. As a result, the TEST average surface free energy reaches 57.24 mN/m, indicating a far more hydrophilic behavior than the REF surface (See Figure 4a and 4b), with an average surface free energy of 33.86 mN/m. Results of these are detailed in Table 3.

3.2   Micro-CT analysis

Comparing both REF and TEST implants by Micro-CT analysis, no statiscal difference appears in terms of BIC and BV/TV (Fig. 5). At 4 weeks after implantation, the BIC reaches 65.1±10.9% on the REF implant at the coronal region, while it attains 61.8±10.8% on the TEST one. At 13 weeks, BIC tends to increase to 74.4±10.6% for the REF implant and significantly increases up to 80.6±7.4% for the TEST one. The BV/TV ratio does not show any evidence of variation over time. Bone response at the apical region shows a significant difference behavior compared to the coronal one at the same time period. Nevertheless, no significant difference in the results at the apical region is observable between the implant and between time periods.

3.3   Histopathologic analysis

Because of an off-axis section, one REF implant was replaced by a reserve one at histology. At 4 weeks (Fig. 6), qualitative analyses of explants did not reveal significant behavior differences in the local tissue impact between the REF and the TEST implants. The defect generated through drilling during the surgical procedure was still visible for both implants, allowing a clear distinction between the host bone and healing chamber, particularly in the apical region of the implant. No marked inflammation was observed, as indicated by only a slight number of macrophages and osteoclasts, admixed with rare lymphocytes and polymorphonuclear cells. Bone marrow formation was observed in 4 out of 10 sites for the REF implant against 7 out of 10 sites for the TEST one. Combined with qualitative observations, these results indicate for both implants a marked woven bone

neoformation, without tangible evidence of bone remodeling. Bone condensation is visible around the implants, especially at the coronal region. Marked signs of bone apposition and moderate to marked osteoconduction is observed, along with a marked presence of active osteoblasts. Bone mineralization activity already started at day 5, reaching a peak at day 15 mostly through bone deposition, then slightly decreased at day 25. At 13 weeks (Fig. 7), while no significative differences were noted in the semi-quantitative bone healing parameters between the REF implant and the TEST one, differences were observed in bone response in terms of architecture. Indeed, for both implants, a decreased number of osteoblasts is noted compared to the 4W group as well as marked signs of bone neoformation, osseointegration and osteoconduction. Consistent bone marrow formation was found and bone mineralization activity was present at a marked level, mostly through bone thickening and surface apposition at week 4 and week 8, before slowing down to a more moderate level at week 12. Nevertheless, the TEST implant showed no more bone condensation but remodeling of the original bone architecture before implantation, with thick bone trabeculae. The defect margins was undistinguishable between host bone and neoformed bone. Regarding the REF implant, the defect margins remained somewhat visible and discreet bone condensation could still be observed, despite a moderate to marked bone remodeling and thick bone trabeculae. Semi-quantitative histopathologic results at week 4 and week 13 are compiled in Appendix A.

3.4   Histomorphometric analysis

Contrary to the Micro-CT evaluation, significant differences were raised up by histomorphometric analyses. Only slight variation of the BIC in the apical region is visible, as it is increasing from 63.5±9.9% to 66.2±14.7% for the REF implant and decreasing from 69.2±10.3% to 64.2±14.6% for the TEST implant, between week 4 and week 13 (Fig. 8).

Table 3: Hydrophilicity assessment through contact angle measurements and surface free energy calculation.

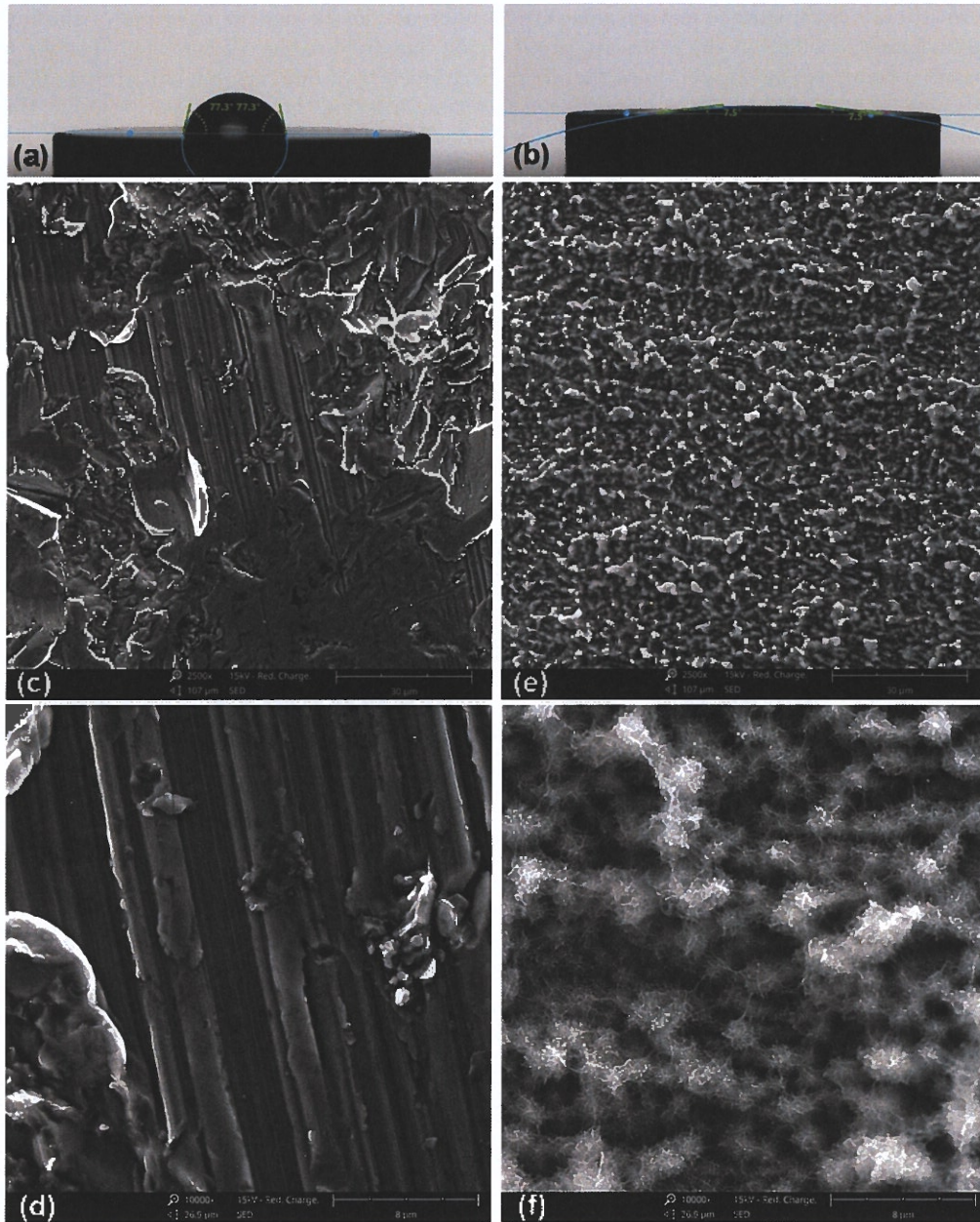|		Contact Angle (°)		Surface Free Energy (mN/m)	
	Liquid	Mean	*SD*	Mean	*SD*
REF	water	77.93	*2.05*	33.86	*5.45*
	ethylene glycol	60.78	*3.44*		
	diiodomethane	57.1	*3.62*		
TEST	water	6.15*	*2.4*	57.24*	*10.3*
	ethylene glycol	3.68*	*0.74*		
	diiodomethane	6.57*	*0.61*		

* $p<0.01$ compared to REF surface.

Figure 4: SEM of implants surface (a,b) REF surface at magnification (a)×2500 and (b) ×10 000; (c,d) TEST surface at magnification (c)×2500 and (d)×10 000.

In the coronal region, the BIC of the REF implant is increasing from 68.3±8.8% to 74.8±13% between week 4 and week 13. BIC results for the TEST implant are significantly higher from the REF one at both week 4 and week 13, as their value are respectively equal to 79.3±11.2% and 86.4±6.7%. No impact of the implant on local tissue densities was observed (Fig. 9). A significant decrease of the fibrous tissue density can however be seen between week 4 and week 13 for both implants, and both at their coronal and apical region. In particular, this decrease leads to a significant difference in fibrous tissue density in favor of the TEST implant at week 13 compared to the REF one, in the apical region. An increase in the implant roughness and hydrophilicity through the presence of micro and nanofeatures improve osseointegration.

4 Discussion

We observe in this study that implants surface modifications are beneficial to bone response in their coronal region. Such results confirm what has already been concluded by the

scientific literature [15–18]. Such surface feature generates an additive, if not synergistic, effect in the adhesion, proliferation and differentiation of osteogenic cell lines therefore leading to an increase in *de novo* bone formation *in vivo*. While the exact mechanisms of bone response
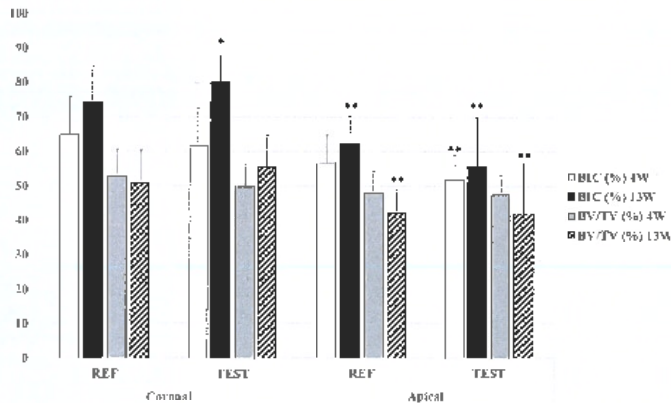

Figure 5: Micro-CT evaluation of BIC (%) and BV/TV (%) at the coronal and apical regions of REF and TEST implants. * *p<0.05* compared to 4W group, ** *p<0.05* compared to coronal group at the same time period.

enhancement in its entireness remain unclear, studies suggest that nanofeatures affect the adsorption and conformation of vitronectin and fibronectin, proteins responsible for the adhesion of osteoblasts, onto the implant surface. Such adhesion would therefore regulate the subsequent proliferation and differentiation of mesenchymal stem cells [14, 32]. The absence of tissue deleterious response for both REF and TEST implants indicates that the implant biocompatibility is preserved despite the topography modifications. Furthermore, it was observed in this study that mineralization activity was not affected by the Starsurf® surface treatment. In a study conducted in dog jaws, Abrahamsson et al. (2004) suggested an increase in lamellar bone formation around dental implants between 2 weeks and 4 weeks after implantation [33], which is similar to the peaks observed for the REF and TEST implants, 15 days after implantation. This same study also emphasized the presence of a front of bone deposition onto the implant surface. Within the limits of a semi-quantitative histopathologic evaluation, it can be deduced that the Starsurf® surface treatment is not deleterious to the bone mineralization activity and moreover promotes osteoconduction. Micro-CT evaluation demonstrated no significant difference between the REF and TEST implants regarding their osseointegration in both coronal and apical regions. This lack of difference, when compared to histomorphometric analyses can be explained by the high interferency generated by titanium implant [34]. These artifacts hinder measurements close to the surface of implants, therefore decreasing the accuracy of such evaluation. However, this evaluation highlights the significant

difference in the osseointegration of the implant apical region compared to the coronal one. This observation could be explained by a different implant thread design at the apical region, altering the stress distribution at the interface with bone [35, 36] and increasing wound chambers dimensions [37], therefore modifying the osteogenic response to the implant [38]. Finally, this study highlights a major difference in the bone architecture around the implants at week 13. While at week 4 similar bone architecture between REF and TEST implants are observed, with bone condensation and presence of the initial defect margins, bone remodeled for the TEST implant in a way that trabeculae recovered their initial connectivity, leaving no detectable trace of the drill made to insert the implant. In addition, trabeculae seem to be oriented towards the threads tips of the implant, where the mechanical stress is significant, and perpendicular to the implant surface. Such observation is in accordance with Wolff's law of bone remodeling [39], from which the concept of "bone functional adaptation" is originated [40], explaining the process of long-term osseointegration. This concept indicates that mechanical load applied to living bone influences the structure of bone tissue over time. Increased local strain results in a greater deposition of bone tissue while decreased strain leads to resorption of bone tissue until restoring the original strain levels of bone, also termed "optimum customary strain level". This study suggests that this optimum was reached more rapidly for the TEST implant compared to the REF one. Osseointegration of TEST implant results in an adequate bone remodeling, close to the original bone architecture. Consequently, the TEST implant is not subject to stress shielding complications, inducing excess of bone
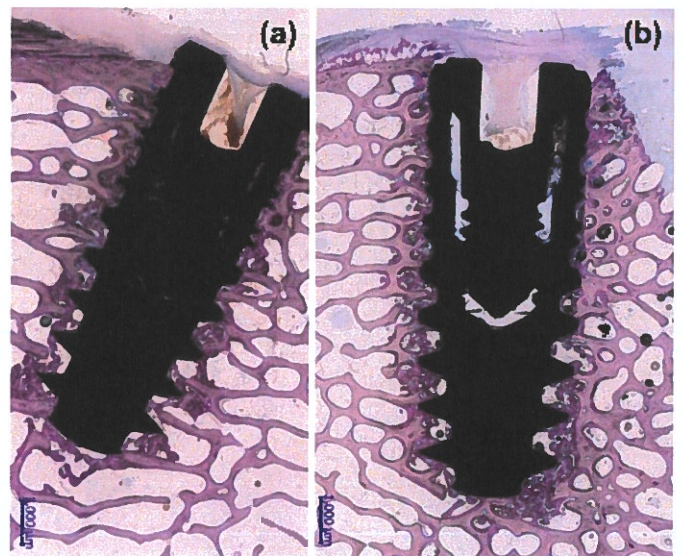

Figure 6: Photomicrograph of a (a) REF implant and (b) TEST implant, 4 weeks after implantation. Bone condensation is visible all around the implant, depicting the initial defect margins created through the drilling surgical procedure.
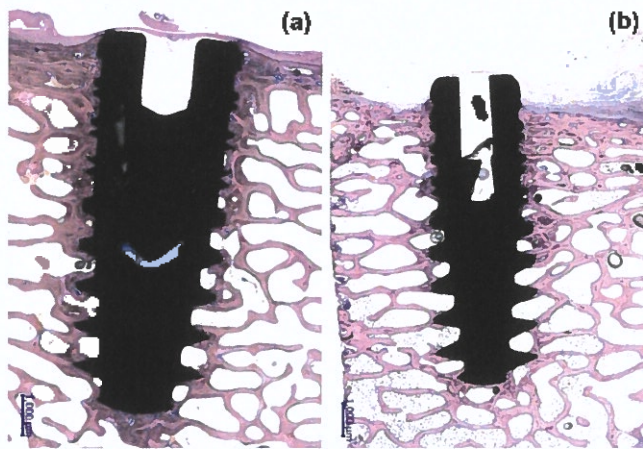
Figure 7: Photomicrograph of a (a) REF implant and (b) TEST implant, 13 weeks after implantation. While defect margins are still visible along with discreet bone condensation around the REF implant, the TEST implant shows a recovery of the original bone architecture, with almost invisible bone condensation and defect margins.

formation in locally overloaded regions and bone resorption in underloaded regions, responsible for implant loosening [41–43]. Furthermore, the TEST implant leads to a geometrically valid architecture. Interestingly, similar patterns were observed in other *in vivo* studies. Perrin et al. (2002) through the insertion of titanium dental implants of various topographies into Land Race pigs mandible observed after 10 weeks a preferential orientation and distribution of bone trabeculae. These trabeculae were oriented perpendicular to the implant surface and located at the thread level of the implant [44]. This behavior was justified with an assertion made by Gross et al. (1990), who through the insertion of titanium cylinders presenting different surface roughness into distal epiphysis of rabbit femurs noticed the formation of a cortical shell around implants with smooth surfaces, opposed to oriented trabeculae with increasing surface roughness [45]. It was suggested that surface roughness promotes bone trabecularization around the implant, leading to a better immobilization of this last. In an animal experiment employing porous coated and proximally partially porous coated femoral canine implants, Bobyn et al. (1987) noted a similar shell around the smooth surface, interposed with a space filled with fibrous tissue [46]. Based on these observations, Luo et al. (1999) affirm through computational methods that such shell is supposed to resorb over time, leading to a trabeculization of the bone-implant interface [47]. These studies tend to correlate the assertion made in the present one. TEST implants topography plays a role in local stress distribution, therefore resulting in a faster recovery of bone original architecture and a better immobilization of the implant.

5   Conclusion

The present study demonstrates that the Starsurf® surface treatment, generating a combination of micro- and nanofeatures on the surface of a titanium implant, has significant beneficial effects on the osseointegration process. Such treatment suggests an increase in the kinetics of bone regeneration and remodeling to the extent that original bone architecture is recovered within 13 weeks, allowing the long-term implant stability. Furthermore, such osseointegration occurs without any deleterious local effect on the surrounding tissue, showing a good compatibility of the implant within its environment. Finally, the distinction between the coronal and apical regions of the implant allowed to demonstrate a difference of bone behavior along the implant, that could be both attributed to the change of implant thread geometry and increasing mechanical stresses generated at the apex.

Acknowledgement

Conflict of Interest

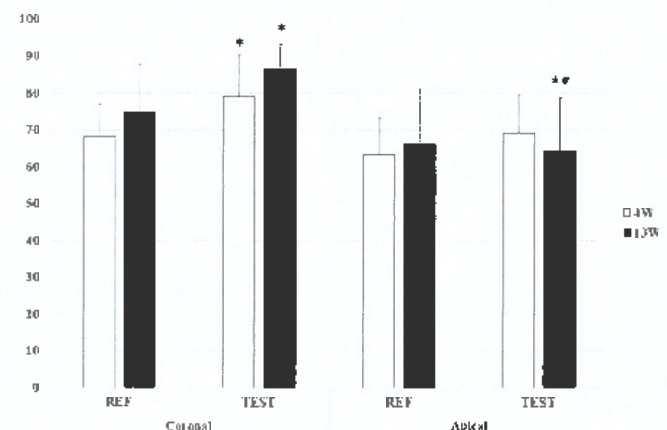No potential conflict of interest was reported by the authors.

Figure 8: Histomorphometric of BIC (%) at the coronal and apical portions of REF and TEST implants.* $p < 0.05$ compared to REF group at the same time period; ** $p < 0.05$ compared to Coronal group for the same implant at the corresponding time period.
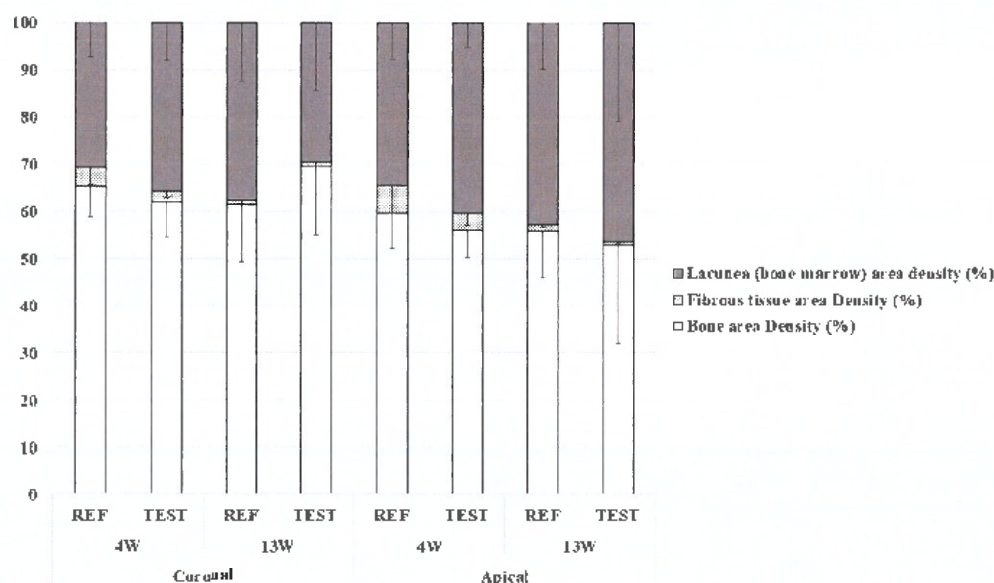
Figure 9: Tissue density evaluation at the coronal and apical regions of REF and TEST implants.

References

[1] P. I. Brånemark, U. Breine, R. Adell, B. O. Hansson, J. Lindström, and A. Ohlsson. "Intra-osseous anchorage of dental prostheses: I. Experimental studies,". *Scandinavian Journal of Plastic and Reconstructive Surgery and Hand Surgery*, 3(2):81–100, 1969. ISSN 02844311. doi: 10.3109/02844316909036699.

[2] A. C. Schroeder, Ortrun E. M. Pohler, and Franz Sutter. "Tissue reaction to an implant of a titanium hollow cylinder with a titanium surface spray layer,". *SSO Schweiz Monatsschr Zahnheilkd*, 86(7):713–27, 1976.

[3] D. Buser, N. Broggini, M. Wieland, R. K. Schenk, A. J. Denzer, D. L. Cochran, B. Hoffmann, A. Lussi, and S. G. Steinemann. "Enhanced bone apposition to a chemically modified SLA titanium surface,". *Journal of Dental Research*, 83(7):529–533, 2004. ISSN 00220345. doi: 10.1177/154405910408300704.

[4] S. Szmukler-Moncler, D. Perrin, V. Ahossi, G. Magnin, and J. P. Bernard. "Biological Properties of Acid Etched Titanium Implants: Effect of Sandblasting on Bone Anchorage,". *Journal of Biomedical Materials Research - Part B Applied Biomaterials*, 68 (2):149–159, 2004. ISSN 00219304. doi: 10.1002/jbm.b.20003.

[5] Zvi Schwartz, Perry Raz, Ge Zhao, Yael Barak, Michael Tauber, Hai Yao, and Barbara D. Boyan. "Effect of micrometer-scale roughness of the surface of Ti6Al4V pedicle screws in vitro and in vivo,". *Journal of Bone and Joint Surgery - Series A*, 90(11): 2485–2498, 2008. ISSN 00219355. doi: 10.2106/JBJS.G.00499.

[6] F. M. He, G. L. Yang, Y. N. Li, X. X. Wang, and S. F. Zhao. "Early bone response to sandblasted, dual acid-etched and H2O2/HCl treated titanium implants: an experimental study in the rabbit,". *International Journal of Oral and Maxillofacial Surgery*, 38(6): 677–681, 2009. ISSN 09015027. doi: 10.1016/j.ijom.2009.03.716.

[7] R. Olivares-Navarrete, P. Raz, G. Zhao, J. Chen, M. Wieland, D. L. Cochran, R. A. Chaudhri, A. Ornoy, B. D. Boyan, and Z. Schwartz. "Integrin alpha2beta1 plays a critical role in osteoblast response to micron-scale surface structure and surface energy of titanium substrates,". *Proceedings of the National Academy*

of Sciences, 105(41):15767–15772, 2008. ISSN 0027-8424. doi: 10.1073/pnas.0805420105.

[8] Ge Zhao, Olivier Zinger, Zvi Schwartz, Marco Wieland, Dieter Landolt, and Barbara D. Boyan. "Osteoblast-like cells are sensitive to submicron-scale surface structure,". *Clinical Oral Implants Research*, 17(3):258–264, 2006. ISSN 09057161. doi: 10.1111/j.1600-0501.2005.01195.x.

[9] Myung-Joo Kim, Chang-Whe Kim, Young-Jun Lim, and Seong-Joo Heo. "Microrough titanium surface affects biologic response in MG63 osteoblast-like cells Myung-Joo,". *Wiley Interscience*, 67 (8):1180–1185, 2016. ISSN 00309982. doi: 10.1002/jbm.a.31040.

[10] Oleh Andrukhov, Rebecca Huber, Bin Shi, Simon Berner, Xiaohui Rausch-Fan, Andreas Moritz, Nicholas D. Spencer, and Andreas Schedle. "Proliferation, behavior, and differentiation of osteoblasts on surfaces of different microroughness,". *Dental Materials*, 32(11):1374–1384, 2016. ISSN 01095641. doi: 10.1016/j.dental.2016.08.217.

[11] Lars M. Bjursten, Lars Rasmusson, Seunghan Oh, Garrett C. Smith, Karla S. Brammer, and Sungho Jin. "Titanium dioxide nanotubes enhance bone bonding in vivo,". *Journal of Biomedical Materials Research - Part A*, 92(3):1218–1224, 2010. ISSN 15493296. doi: 10.1002/jbm.a.32463.

[12] R. Jimbo, Y. Xue, M. Hayashi, H. O. Schwartz-Filho, M. Andersson, K. Mustafa, and A. Wennerberg. "Genetic responses to nanostructured calcium-phosphate-coated implants,". *Journal of Dental Research*, 90(12):1422–1427, 2011. ISSN 00220345. doi: 10.1177/0022034511422911.

[13] Thomas J. Webster, Celaletdin Ergun, Robert H. Doremus, Richard W. Siegel, and Rena Bizios. "Specific proteins mediate enhanced osteoblast adhesion on nanophase ceramics,". *Journal of Biomedical Materials Research*, 51(3):475–483, 2000. ISSN 00219304. doi: 10.1002/1097-4636(20000905)51:3<475::aid-jbm23>3.0.co;2-9.

[14] Jung Park, Sebastian Bauer, Karl Andreas Schlegel, Friedrich W. Neukam, Klaus Der Von Mark, and Patrik Schmuki. "TiO2

nanotube surfaces: 15 nm - an optimal length scale of surface topography for cell adhesion and differentiation,". *Small*, 5(6): 666–671, 2009. ISSN 16136810. doi: 10.1002/smll.200801476.

[15] Rolando A. Gittens, Taylor McLachlan, Rene Olivares-Navarrete, Ye Cai, Simon Berner, Rina Tannenbaum, Zvi Schwartz, Kenneth H. Sandhage, and Barbara D. Boyan. "The effects of combined micron-/submicron-scale surface roughness and nanoscale features on cell proliferation and differentiation,". *Biomaterials*, 32 (13):3395–3403, 2011. ISSN 01429612. doi: 10.1016/j.biomaterials. 2011.01.029.

[16] Rolando A. Gittens, Rene Olivares-Navarrete, Alice Cheng, David M. Anderson, Taylor McLahan, Ingrid Stephan, Jürgen Geis-Gerstorfer, Kenneth H. Sandhage, Andrei G. Fedorov, Frank Rupp, Barbara D. Boyan, Rina Tannenbaum, and Zvi Schwartz. "The Roles of Titanium Surface Micro/Nanotopography and Wettability on the Differential Response of Human Osteoblast Lineage Cells,". *Acta Biomaterialia*, 9(4):6268–6277, 2013. doi: 10.1016/j.actbio.2012.12.002.

[17] Lingzhou Zhao, Shenglin Mei, Paul K. Chu, Yumei Zhang, and Zhifen Wu. "The influence of hierarchical hybrid micro/nano-textured titanium surface with titania nanotubes on osteoblast functions,". *Biomaterials*, 31(19):5072–5082, 2010. ISSN 01429612. doi: 10.1016/j.biomaterials.2010.03.014.

[18] Katsutoshi Kubo, Naoki Tsukimura, Fuminori Iwasa, Takeshi Ueno, Lei Saruwatari, Hideki Aita, Wen An Chiou, and Takahiro Ogawa. "Cellular behavior on TiO2 nanonodular structures in a micro-to-nanoscale hierarchy model,". *Biomaterials*, 30(29):5319–5329, 2009. ISSN 01429612. doi: 10.1016/j.biomaterials.2009.06. 021.

[19] Liwen Lin, Hui Wang, Ming Ni, Yunfeng Rui, Tian Yuan Cheng, Cheng Kung Cheng, Xiaohua Pan, Gang Li, and Changjian Lin. "Enhanced osteointegration of medical titanium implant with surface modifications in micro/nanoscale structures,". *Journal of Orthopaedic Translation*, 2(1):35–42, 2014. ISSN 2214031X. doi: 10.1016/j.jot.2013.08.001.

[20] Yada Li, Weiqiang Wang, Huiying Liu, Jingwu Lei, Jingying Zhang, Hongzhi Zhou, and Min Qi. "Formation and in vitro/in vivo performance of "cortex-like" micro/nano-structured TiO2 coatings on titanium by micro-arc oxidation,". *Materials Science and Engineering C*, 87:90–103, 2018. ISSN 09284931. doi: 10.1016/j.msec.2018.02.023.

[21] Yongfeng Li, Yuan Gao, Bo Shao, Jianrui Xiao, Kaijin Hu, and Liang Kong. "Effects of hydrofluoric acid and anodised micro and micro/nano surface implants on early osseointegration in rats,". *British Journal of Oral and Maxillofacial Surgery*, 50(8):779–783, 2012. ISSN 02664356. doi: 10.1016/j.bjoms.2011.12.008.

[22] Fuwei Liu, Yongfeng Li, Jianfei Liang, Wen Sui, Anuj Bellare, and Liang Kong. "Effects of micro/nano strontium-loaded surface implants on osseointegration in ovariectomized sheep,". *Clinical Implant Dentistry and Related Research*, 21(2):377–385, 2019. ISSN 17088208. doi: 10.1111/cid.12719.

[23] SELENIUM MEDICAL. "Internal validation protocol Q021044SV000_002 - Performance Qualification_Micro-Starsurf & Starsurf Process,". .

[24] SELENIUM MEDICAL. "Internal validation protocol Q021044SV000_001 v01 - Operational Qualification_ Micro-StarSurf & StarSurf Process,". .

[25] Katja M.R. Nuss, Joerg A. Auer, Alois Boos, and Brigitte Von Rechenberg. "An animal model in sheep for biocompatibility testing of biomaterials in cancellous bones,". *BMC Musculoskeletal*

[26] Suelen Cristina Sartoretto, Marcelo José Uzeda, Fúlvio Borges Miguel, Jhonathan Raphaell Nascimento, Fabio Ascoli, and Mônica Diuana Calasans-Maia. "Sheep as an experimental model for biomaterial implant evaluation,". *Acta Ortopedica Brasileira*, 24(5):262–266, 2016. ISSN 14137852. doi: 10.1590/1413-785220162405161949.

[27] A. I. Pearce, R. G. Richards, S. Milz, E. Schneider, and S. G. Pearce. "Animal models for implant biomaterial research in bone: A review,". *European Cells and Materials*, 13:1–10, 2007. ISSN 14732262. doi: 10.22203/eCM.v013a01.

[28] International Organization for Standardization. "EN/ISO 10993-6 : Tests for Local Effects after implantation,", 2016.

[29] NAMSA. "Final GLP Report 263585 : Local Tissue Effects and Performance of Four Titanium Implants Following Intra-Osseous Implantation in the Sheep,". Technical report, 2019.

[30] Carol Kilkenny, William J. Browne, Innes C. Cuthill, Michael Emerson, and Douglas G. Altman. "Improving bioscience research reporting: The arrive guidelines for reporting animal research,". *PLoS Biology*, 8(6):8–9, 2010. ISSN 15449173. doi: 10.1371/journal.pbio.1000412.

[31] B. Guillaume. "Dental implants : a review,". *Morphologie*, 100 (331):189–198, 2016. ISSN 12860115. doi: 10.1016/j.morpho.2016. 02.002.

[32] Andrés J. García, María D. Vega, and David Boettiger. "Modulation of Cell Proliferation and Differentiation through Substrate-dependent Changes in Fibronectin Conformation,". *Molecular Biology of the Cell*, 10(3):785–798, 1999. doi: 10.1091/mbc.10.3.785.

[33] Ingemar Abrahamsson, Tord Berglundh, Elena Linder, Niklaus P. Lang, and Jan Lindhe. "Early bone formation adjacent to rough and turned endosseous implant surfaces. An experimental study in the dog,". *Clinical Oral Implants Research*, 15(4):381–392, 2004. ISSN 09057161. doi: 10.1111/j.1600-0501.2004.01082.x.

[34] Shuo Liu, Joseph Broucek, Amarjit S. Virdi, and D. Rick Sumner. "Limitations of Using Micro Computed Tomography to Predict Bone-Implant Contact and Mechanical Fixation,". *Journal of Microscopy*, 245(1):34–42, 2012. doi: 10.1111/j.1365-2818.2011.03541.x.

[35] Heba Abuhussein, Giorgio Pagni, Alberto Rebaudi, and Hom Lay Wang. "The effect of thread pattern upon implant osseointegration: Review,". *Clinical Oral Implants Research*, 21(2):129–136, 2010. ISSN 09057161. doi: 10.1111/j.1600-0501.2009.01800.x.

[36] Jennifer Steigenga, Khalaf Al-Shammari, Carl Misch, Francisco H. Nociti, and Hom-Lay Wang. "Effects of Implant Thread Geometry on Percentage of Osseointegration and Resistance to Reverse Torque in the Tibia of Rabbits,". *Journal of Periodontology*, 75(9):1233–1241, 2004. ISSN 0022-3492. doi: 10.1902/jop.2004.75.9.1233.

[37] Charles Marin, Rodrigo Granato, Marcelo Suzuki, Jose N. Gil, Malvin N. Janal, and Paulo G. Coelho. "Histomorphologic and histomorphometric evaluation of various endosseous implant healing chamber configurations at early implantation times: A study in dogs,". *Clinical Oral Implants Research*, 21(6):577–583, 2010. ISSN 09057161. doi: 10.1111/j.1600-0501.2009.01853.x.

[38] J Davies. "Understanding peri-implant endosseous healing.,". *Journal of dental education*, 67(8):932–949, 2003. ISSN 0022-0337.

[39] Julius Wolff. "Das gesetz der transformation der knochen,". *Berlin : Quarto*, 1892.

[40] L. E. Lanyon, A. E. Goodship, C. J. Pye, and J. H. MacFie. "Mechanically adaptive bone remodelling.". *Journal of Biomechanics*, 15(3):141–154, 1982. ISSN 00219290. doi: 10.1016/0021-9290(82)90246-9.

[41] H. M. Frost. "Wolff's Law and bone's structural adaptations to mechanical usage: an overview for clinicians.". *Angle Orthodontist*, 64(3):175–188, 1994. ISSN 00033219. doi: 10.1043/0003-3219(1994)064<0175:WLABSA>2.0.CO;2.

[42] Christopher Ruff, Brigitte Holt, and Erik Trinkaus. "Who's Afraid of the Big Bad Wolff ? : "Wolff's Law" and Bone Functional Adaptation,". *American Journal of Physical Anthropology*, 129(4): 484–498, 2006. ISSN 10601538. doi: 10.1002/ajpa.

[43] M. I.Z. Ridzwan, Solehuddin Shuib, A. Y. Hassan, A. A. Shokri, and M. N. Mohammad Ibrahim. "Problem of stress shielding and improvement to the hip implant designs: A review,". *Journal of Medical Sciences*, 7(3):460–467, 2007. ISSN 18125727. doi: 10.3923/jms.2007.460.467.

[44] Daniel Perrin, Serge Szmukler-Moncler, Casimir Echikou, Philippe Pointaire, and Jean Pierre Bernard. "Bone response to alteration of surface topography and surface composition of sandblasted and acid etched (SLA) implants,". *Clinical Oral Implants Research*, 13(5):465–469, 2002. ISSN 09057161. doi: 10.1034/j.1600-0501.2002.130504.x.

[45] U. Gross, C. Müller-Mai, T. Fritz, C. Voigt, W. Knarse, and H. J. Schmitz. "Implant surface roughness and mode of load transmission influence peri implant bone structure,". *Clinical Implant Materials (Advances in Biomaterials)*, 9:303–308, 1990.

[46] J. D. Bobyn, R. M. Pilliar, A. G. Binnington, and J. A. Szivek. "The effect of proximally and fully porous-coated canine hip stem design on bone modeling,". *Journal of Orthopaedic Research*, 5 (3):393–408, 1987. ISSN 1554527X. doi: 10.1002/jor.1100050312.

[47] Gangming Luo, Ali M. Sadegh, Harold Alexander, William Jaffe, David Scott, and Stephen C. Cowin. "The effect of surface roughness on the stress adaptation of trabecular architecture around a cylindrical implant,". *Journal of Biomechanics*, 32(3):275–284, 1999. ISSN 00219290. doi: 10.1016/S0021-9290(98)00172-9.

Appendix A. Results of semi-quantitative histopathologic analysis

Time period	4W				13W			
	REF		TEST		REF		TEST	
Implant	Mean	SD	Mean	SD	Mean	SD	Mean	SD
Polymorphonuclear cells	0.1	0.3	0.0	0.0	0.0	0.0	0.0	0.0
Lymphocytes	0.4	0.5	0.4	0.9	0.3	0.5	0.3	0.5
Plasma cells	0.0	0.0	0.0	0.0	0.0	0.0	0.0	0.0
Macrophages	1.0	0.0	1.1	0.3	1.0	0.0	1.2	0.4
Giant cells/osteoclastic cells	1.0	0.0	1.2	0.6	1.1	0.3	1.0	0.0
Necrosis	0.0	0.0	0.0	0.0	0.0	0.0	0.0	0.0
Osteolysis	0.0	0.0	0.2	0.6	0.0	0.0	0.0	0.0
Neovascularization	2.3	0.5	2.3	0.5	2.0	0.0	2.1	0.3
Fatty infiltrate/bone marrow	1.1	0.8	1.6	0.7	2.7	0.5	2.6	0.7
Fibrin	0.4	0.7	0.1	0.3	0.0	0.0	0.0	0.0
Hemorrhage	0.2	0.6	0.0	0.0	0.0	0.0	0.0	0.0
Cell or tissue degeneration	0.0	0.0	0.0	0.0	0.0	0.0	0.0	0.0
Fibroplasia	1.0	0.8	0.6	0.5	0.6	0.5	0.3	0.5
Encapsulation	0.0	0.0	0.0	0.0	0.0	0.0	0.0	0.0
Fibrosis	0.1	0.3	0.0	0.0	0.3	0.5	0.0	0.0
Osteoblastic cells	2.8	0.4	2.9	0.3	1.8	0.4	1.8	0.4
Bone neoformation	2.8	0.4	2.8	0.4	3.2	0.4	3.3	0.5
Osteoconduction	2.6	0.5	2.7	0.5	3.1	0.3	3.2	0.4
Osteointegration	2.8	0.4	2.9	0.3	3.0	0.0	3.1	0.3
Bone remodeling	0.0	0.0	0.0	0.0	2.7	0.5	3.0	0.0
Material degradation	0.0	0.0	0.0	0.0	0.0	0.0	0.0	0.0
Bone mineralization XO[1]	1.4	0.5	1.5	0.5	3.4	0.5	3.3	0.5
Bone mineralization CG[2]	3.5	0.5	3.5	0.7	3.1	0.3	3.2	0.4
Bone mineralization OTC[3]	2.8	0.4	2.7	0.5	2.6	0.5	2.0	0.0

Scoring scale : 0 = None; 1 = Slight; 2 = Moderate; 3 = Marked; 4 = Severe
[1] : 4W group = 5 days; 13W group = 4 weeks
[2] : 4W group = 15 days; 13W group = 8 weeks
[3] : 4W group = 25 days; 13W group = 12 weeks